

---

---

Original article

## Energy Flows between the Mean Currents and the Mesoscale Eddies in the Eastern and Western Parts of the Black Sea

A. A. Pavlushin

*Marine Hydrophysical Institute of RAS, Sevastopol, Russian Federation*

✉ [pavlushin@mhi-ras.ru](mailto:pavlushin@mhi-ras.ru)

### Abstract

**Purpose.** The study consists in analyzing the energy flows between the currents of different scales in the eastern and western parts of the Black Sea.

**Methods and Results.** The energy balance components were determined based on the results of numerical calculation of current fields in the Black Sea performed using a two-layer eddy-resolving model subjected to a forcing of a wind with cyclonic vorticity. A complete non-stationary large-scale sea circulation was represented conventionally as a sum of mean currents and mesoscale eddies. Conversions between the kinetic and available potential energy, as well as the energy flows between the mean currents and the mesoscale eddies were calculated separately for the eastern and western parts of the Black Sea. Besides, the advective energy flows across the meridional boundary between two parts of the sea were also calculated.

**Conclusions.** The main contribution to the potential energy advective transfer from the eastern part of the Black Sea to its western part is made by the mesoscale eddies. This advective energy transfer results in arising of differences in the energy flow directions in the currents of different scales in the eastern and western parts of the sea. In the Black Sea eastern part, energy is transferred from the mean currents to the mesoscale eddies, whereas in its western part, a reverse energy flow is observed. It is shown that the kinetic energy exchange between the movements of different scales is provided by the Coriolis force work, which for the initial currents is equal to zero, but turns out to be non-zero separately for the mean flows and the mesoscale eddies.

**Keywords:** Black Sea, large-scale circulation, mean currents, mesoscale eddies, energy balance, energy flow,  $\beta$ -effect, Rossby waves

**Acknowledgements:** The study was carried out within the framework of state assignment FNNN-2022-0003 “Development of operational oceanology methods based on interdisciplinary research of the processes of marine environment formation and evolution, and mathematical modelling using the data of remote and contact measurements”.

**For citation:** Pavlushin, A.A., 2024. Energy Flows between the Mean Currents and the Mesoscale Eddies in the Eastern and Western Parts of the Black Sea. *Physical Oceanography*, 31(1), pp. 99-119.

© 2024, A. A. Pavlushin

© 2024, Physical Oceanography

### Introduction

Interaction among dynamic processes of various scales plays an important role in the formation and variability of horizontal water circulation in the oceans and seas. According to the classification by A.S. Monin<sup>1</sup>, variability of interannual, seasonal and synoptic scales is relevant for the Black Sea circulation. Processes on

---

<sup>1</sup> Monin, A.S., Kamenkovich, V.M. and Kort, V.G., 1977. *Variability of the Oceans*. New York, London, Sydney, Toronto: John Wiley & Sons, 241 p.



an interannual and seasonal scale appear in the formation of currents limited by the basin size. In the Black Sea, there is the Rim Current which in some years spreads along the entire perimeter of the deep water and in other years breaks up into two or three sub-basin cyclonic gyres called “Knipovich glasses” [1]. Synoptic-scale processes include the Rim Current meanders, anticyclonic and cyclonic eddies formed in meander troughs, rings – detached meanders, quasi-stationary anticyclones (Sevastopol, Batumi) and Rossby waves with scales on the order of the baroclinic deformation radius [2, 3].

In [4–6], when describing the features of current fields, foreign authors use another classification more often. According to it, eddy formations, which, according to A. S. Monin’s definition, are synoptic [7], are classified as mesoscale objects. Such objects, from ten to several hundred kilometers in size, are called mesoscale eddies and their lifetime ranges from a week to several months [8]. Respectively, phenomena of a larger scale than mesoscale eddies are classified as large-scale, while phenomena of a smaller scale are classified as submesoscale. In the present paper, submesoscale dynamic objects are not considered, since the spatial resolution of the two-layer eddy-resolving model [9] used to calculate the fields of hydrophysical characteristics does not make it possible. In the future, some modernization of the model is planned in order to increase its spatial resolution so that to study the influence of submesoscale processes on larger scale ones, since this issue is of scientific interest [10–12].

For reasons of presentation, in this work we use the division of processes into large-scale and mesoscale ones, as it is customary in foreign literature. Mean currents (MCs) obtained by time averaging of instantaneous current fields are considered as large-scale ones, and deviations of instantaneous currents from this average state are eddy formations, more often called mesoscale eddies (MEs). In the Black Sea, mesoscale eddies are formed mainly due to the hydrodynamic instability of large-scale currents [13]. They participate in the energy transfer into the deep layers, influence the wind energy inflow and horizontal mixing of waters [14].

To study the Black Sea dynamics, the method of energy analysis is applied. It implies calculation and estimation of the energy parameters of currents: kinetic energy and potential energy, energy flows (transitions) among different types of energy and scales of movement, sources and sinks of energy. Knowledge of the energy of the considered processes is necessary for a better and correct understanding of their physics [15, 16].

### **Problem statement and description of the model**

This paper aims to study the mutual transitions of kinetic and potential energy caused by large-scale and mesoscale dynamic processes in the Black Sea. At this stage of research, the aim was to calculate and analyze the average transitions of mechanical energy over a long time period among its various types and among movements of various scales separately for the eastern and western parts of the Black

Sea. Division of the sea into two halves was carried out along conventional boundary  $D$ , which coincides with the meridian passing through Cape Sarych (Fig. 1,  $a$ ).

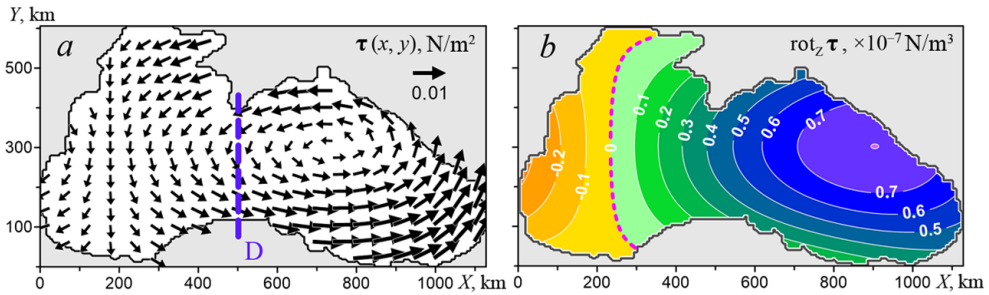


**Fig. 1.** Fields of tangential wind stress ( $a$ ) and vorticity  $\tau$  ( $b$ )

In previous work [17], also devoted to the analysis of the Black Sea energy, it was found that under the influence of the  $\beta$ -effect, an average advective transfer of potential energy was formed from the eastern half of the sea to the western one, resulting in spatial unevenness in the distribution of energy characteristics over the sea area. In the work, time-averaged integral flows and energy transitions in the western and eastern parts of the sea were analyzed, but they were not separated in accordance with the movement scale.

As initial data for calculating the energy characteristics, both in the previous work and in the present one, the results of numerical modelling of the Black Sea circulation using a two-layer eddy-resolving model [9] were used. This model takes into account the real bottom topography, friction at the interface between layers, bottom friction and horizontal turbulent viscosity.

Despite the apparent simplicity, the model used takes into account all the main factors that determine the formation and variability of the current field. With the correct choice of external and internal parameters, the model quite adequately simulates the known features of the large-scale Black Sea circulation – the Black Sea Rim Current with meanders and closely associated mesoscale eddy formations, Batumi and Sevastopol quasi-stationary anticyclones, “Knipovich glasses”, etc. Currents in the lower layer obtained using a two-layer model [18] correspond to observational data of deep currents in the Black Sea [19, 20].

If a stationary or periodically changing wind is used to excite motion in the model, then it is possible to obtain the model solution reaching a statistically equilibrium regime, in which the average values of all calculated characteristics and parameters of the model remain constant.

The model is based on a system of shallow water equations for a two-layer liquid and includes equations of motion and continuity for each layer:

$$(U_1)_t + (U_1 u_1)_x + (V_1 u_1)_y - fV_1 = gh_1 \zeta_x + \tau^x - R_{L1}^x + A_B h_1 (\Delta \Delta u_1),$$

$$(V_1)_t + (U_1 v_1)_x + (V_1 v_1)_y + fU_1 = gh_1 \zeta_y + \tau^y - R_{L1}^y + A_B h_1 (\Delta \Delta v_1),$$

$$(h_1)_t + (U_1)_x + (V_1)_y = 0,$$

$$(U_2)_t + (U_2 u_2)_x + (V_2 u_2)_y - fV_2 = gh_2 \zeta_x + g'h_2 (h_1)_x + R_{L2}^x - R_D^x + A_B h_2 (\Delta \Delta u_2),$$

$$(V_2)_t + (U_2 v_2)_x + (V_2 v_2)_y + fU_2 = gh_2 \zeta_y + g'h_2 (h_1)_y + R_{L2}^y - R_D^y + A_B h_2 (\Delta \Delta v_2),$$

$$(h_2)_t + (U_2)_x + (V_2)_y = 0,$$

where subscripts 1, 2 indicate the layer number; subscripts  $t$ ,  $x$ ,  $y$  mean differentiation with respect to the corresponding variable;  $(u_1, v_1)$ ,  $(u_2, v_2)$  are horizontal components of current velocity in the upper and lower layers, directed along the  $X$  (east) and  $Y$  (north) axes;  $h_1, h_2$  are layer thicknesses;  $\zeta$  is sea level;  $\tau^x, \tau^y$  are components of the tangential wind stress acting on the sea surface;  $(U_1 = u_1 h_1, V_1 = v_1 h_1)$ ,  $(U_2 = u_2 h_2, V_2 = v_2 h_2)$  are components of flows in layers;  $(R_{L1}^x, R_{L1}^y)$ ,  $(R_{L2}^x, R_{L2}^y)$  are friction force components at the lower boundary of the upper layer and the upper boundary of the lower layer, respectively (at the liquid boundary between the layers  $R_{L1}^x = -R_{L2}^x, R_{L1}^y = -R_{L2}^y$ );  $(R_D^x, R_D^y)$  are bottom friction components in the lower layer;  $f = f_0 + \beta y$  is Coriolis parameter,  $f_0 = 10^{-4}$  1/s,  $\beta = 2 \cdot 10^{-8}$  1/(s·m);  $g = 9.81 \text{ m/s}^2$  is free fall acceleration;  $g' = g(\rho_2 - \rho_1)/\rho_2 = 0.032 \text{ m/s}^2$  is reduced gravitational acceleration,  $\rho_1, \rho_2$  is water density in the upper and lower layers;  $A_B$  is coefficient of biharmonic horizontal turbulent viscosity;  $\Delta = \frac{\partial^2}{\partial x^2} + \frac{\partial^2}{\partial y^2}$  is two-dimensional Laplace operator.

To close the system of equations, the model uses the continuity equation for total flows in the rigid-lid approximation  $U_x + V_y = 0$ , where  $U = U_1 + U_2, V = V_1 + V_2$  is components of total flows. This makes it possible to introduce the integral stream function  $\psi$ , for which  $U = -\psi_y, V = \psi_x$ .

River runoff and water exchange through straits are not taken into account in the model; no-slip conditions are set at the lateral boundaries of the basin:  $\mathbf{u}_1 = 0, \mathbf{u}_2 = 0$ .

Since the biharmonic operator is used to parameterize horizontal turbulent viscosity in the model, it becomes necessary to determine the boundary conditions for the Laplacian of current velocity. By analogy with the  $\mathbf{u}_1, \mathbf{u}_2$  conditions  $\Delta \mathbf{u}_1 = 0, \Delta \mathbf{u}_2 = 0$  are set, yet with no physical sense.

Due to weak dissipativity, the model simulates well mesoscale eddies along with large-scale currents which, according to the results of the experiments, permits

to identify the shares of energy and work of forces associated with MCs and MEs. The analysis technique described in [21] makes it possible to calculate energy transitions during the interaction of mesoscale eddies and large-scale currents.

Initial data for calculating the energy characteristics are the fields of the thickness of the upper layer, sea level and current velocities in the upper and lower layers for 30 years with a discreteness of 1 day. The data were obtained in a numerical experiment with the following model parameters: horizontal cell size  $\Delta x = \Delta y = 3000$  m, time integration step  $\Delta t = 120$  s, upper layer thickness at rest  $h_0 = 100$  m, horizontal turbulent viscosity coefficient  $A_B = 2.0 \cdot 10^8$  m<sup>4</sup>/s, bottom friction coefficient  $r_D = 0.002$ , friction coefficient between layers  $r_L = 2.0 \cdot 10^{-6}$  m/s.

The wind effect was set by stationary field of tangential wind stress  $\tau(x, y)$  with an area-variable vorticity (Fig. 1, *a, b*), while the average vorticity over the sea area was cyclonic and amounted to  $0.3 \cdot 10^{-7}$  N/m<sup>3</sup>. The choice of stationary field  $\tau$  is explained by the fact that in this case the numerical model reaches a statistically equilibrium regime quickly.

Fig. 2 shows sea level fields  $\zeta(x, y)$  obtained as a result of calculations characteristic of the statistically equilibrium regime, as well as Montgomery potential  $M(x, y)$  – a function that characterizes the pressure at the interface of the layers<sup>2</sup>. Due to the quasi-geostrophic nature of movements at the considered scale, the spatial distribution of  $\zeta$  and  $M$  gives good indication of large-scale and mesoscale currents. In the upper layer, water moves along the  $\zeta$  isolines, in the lower one – along the  $M$  isolines. The water moves in such a way that greater pressure is to the right of the current direction. The denser the isolines are, the greater the water flow velocity is.

The instantaneous field  $\zeta$  (Fig. 2, *a*) shows the known features of the Black Sea circulation clearly. In the upper layer, the meandering Rim Current and mesoscale anticyclonic eddies to its right are observed. In the lower layer (Fig. 2, *b*), the movement of water has the cyclonic direction in the same way as in the upper layer, though at a lower speed (this can be seen from the span of the  $M$  scale). The circular current in the lower layer meanders strongly, and the meanders extend along the isobaths and move in a counterclockwise direction as the waves captured by the continental slope [9].

The next two fields (Fig. 2, *c, d*) were obtained by averaging the instantaneous fields  $\zeta$ ,  $M$  over a long period of time. They reflect large-scale circulation in the basin. According to the figure, in the upper layer the MC is a circular current located above the continental slope (middle Rim Current), and in the lower layer it is a current in which the current lines are close to the isobaths.

---

<sup>2</sup> Shakina, N.P., 2013. [*Lectures on Dynamic Meteorology*]. Moscow: Triada Ltd., 160 p. (in Russian).

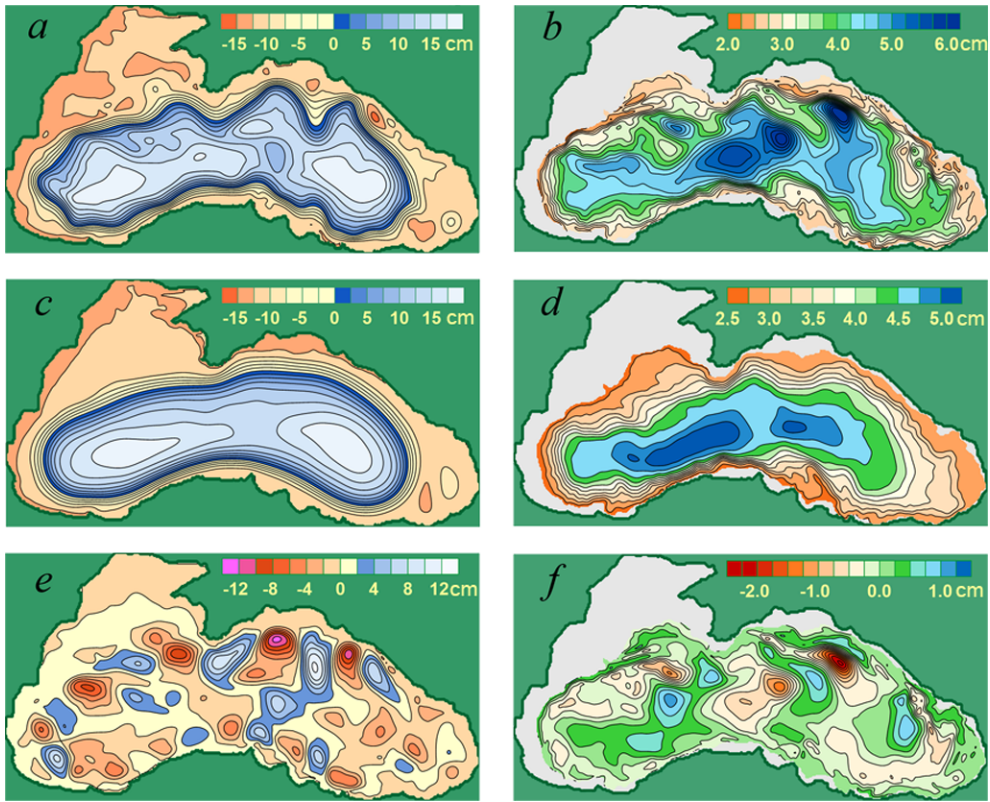


**Fig. 2.** Instantaneous fields  $\zeta$  (a) and  $M$  (b), average fields  $\bar{\zeta}$  (c) and  $\bar{M}$  (d), deviations of the instantaneous values from the average ones  $\zeta - \bar{\zeta}$  (e) and  $M - \bar{M}$  (f)

Fig. 2, *e, f* shows the deviations of instantaneous fields  $\zeta$ ,  $M$  from the average ones. Eddy structures in the lower and upper layers of the sea are clearly visible in it. These eddy formations are interconnected and move in the cyclonic direction with the same phase velocity [20].

### Mechanical energy balance in a two-layer model

The two-layer eddy-resolving model used in the paper is energetically balanced and makes it possible to describe the processes of mechanical energy exchange between the upper and lower layers in a fairly simple form. Mechanical energy in the two-layer model consists of the kinetic energy of currents in individual layers and potential energy.

The kinetic energy of a water column of a unit cross section in upper and lower layers  $K_1$ ,  $K_2$  is determined as follows:

$$K_1 = h_1 e_{K1}, \quad K_2 = h_2 e_{K2}, \quad e_{K1} = \rho_1 \frac{u_1^2 + v_1^2}{2}, \quad e_{K2} = \rho_2 \frac{u_2^2 + v_2^2}{2},$$

where  $e_{K1}$ ,  $e_{K2}$  is kinetic energy per unit volume of water in the upper and lower layers;  $\rho_1$ ,  $\rho_2$  is water density in the layers.

The potential energy of a water column position of a unit cross section from the sea surface to the bottom is equal to

$$PE = -\int_{\zeta}^H \rho(z)gzdz = -\int_{\zeta}^{h_1+\zeta} \rho_1gzdz - \int_{h_1+\zeta}^H \rho_2gzdz = \rho_2 \left( -g \frac{H^2}{2} + g \frac{\zeta^2}{2} + g' \frac{(h_1 + \zeta)^2}{2} - g' \frac{\zeta^2}{2} \right),$$

where  $H(x, y)$  is sea depth.

Vertical coordinate axis  $Z$  is directed downward; the undisturbed sea surface is taken as the origin ( $z = 0$ ). In this case, the potential energy is negative and equal to the work that should be carried out to raise all the water to zero level.

It is more convenient sometimes to use available potential energy ( $P$ ), which is the difference between the current potential energy ( $PE$ ) and the energy of the most stable state of the liquid ( $P_0$ ), instead of potential energy. For a two-layer liquid, the most stable state is the state of rest, in which the sea surface and the interface between the layers are horizontal, therefore

$$P = PE - P_0 = \rho_2 \left( g \frac{\zeta^2}{2} + g' \frac{h_1^2}{2} + g'h_1\zeta - g' \frac{h_0^2}{2} \right),$$

where  $h_0$  is upper layer thickness at rest.

$$\text{In the rigid-lid approximation } P = \rho_2 g' \frac{(h_1^2 - h_0^2)}{2}.$$

The two-layer model energy is described by a system of energy balance equations, consisting of two equations for kinetic energy (upper and lower layers) and an equation for potential energy. Energy balance equations  $K_1$  and  $K_2$  can be obtained by adding up the equations of motion for each layer multiplied by the corresponding components of the current velocity. The potential energy balance equation is obtained by differentiating the equation for  $P$  with respect to time and then using the Boussinesq and rigid-lid approximations:

$$\begin{cases} \frac{\partial K_1}{\partial t} + \frac{\partial U_1 e_{K1}}{\partial x} + \frac{\partial V_1 e_{K1}}{\partial y} = W_{C1} + W_{G1} + W_{\tau} + W_{RL1} + W_{AB1}, \\ \frac{\partial K_2}{\partial t} + \frac{\partial U_2 e_{K2}}{\partial x} + \frac{\partial V_2 e_{K2}}{\partial y} = W_{C2} + W_{G2} + W_{RL2} + W_{RD} + W_{AB2}, \\ \frac{\partial P}{\partial t} - \rho g' \left( \frac{\partial U_2 h_1}{\partial x} + \frac{\partial V_2 h_1}{\partial y} \right) - \rho g \left( \frac{\partial U \zeta}{\partial x} + \frac{\partial V \zeta}{\partial y} \right) = -W_{G1} - W_{G2}, \end{cases} \quad (1)$$

where  $W_{C1} = U_1 \cdot f v_1 - V_1 \cdot f u_1 = 0$ ;  $W_{C2} = U_2 \cdot f v_2 - V_2 \cdot f u_2 = 0$ ;

$W_{\tau} = \rho(u_1 \tau^x + v_1 \tau^y)$ ;

$W_{RL1} = \rho(u_1 R_{L1}^x + v_1 R_{L1}^y)$ ;  $W_{RL2} = \rho(u_2 R_{L2}^x + v_2 R_{L2}^y)$ ;  $W_{RD} = \rho(u_2 R_D^x + v_2 R_D^y)$ ;

$W_{G1} = \rho g(U_1 \zeta_x + V_1 \zeta_y)$ ;  $W_{G2} = \rho g(U_2 \zeta_x + V_2 \zeta_y) + \rho g'(U_2 h_{1x} + V_2 h_{1y})$ ;

$W_{AB1} = \rho A_B(U_1(\Delta \Delta u_1) + V_1(\Delta \Delta v_1))$ ;  $W_{AB2} = \rho A_B(U_2(\Delta \Delta u_2) + V_2(\Delta \Delta v_2))$ ;

$\rho$  is mean water density in the Black Sea.

The left side of equations (1) includes local derivatives with respect to time and divergence of advective flows of corresponding energies.

The right side includes the terms that describe the work per time (power) unit of the forces from the equations of motion, determining corresponding energy flows:  $W_{C1}$ ,  $W_{C2}$  is Coriolis force work in the upper and lower layers;  $W_t$  is tangential wind stress work, equal to kinetic energy influx into the sea (wind pumping);  $W_{RL1}$ ,  $W_{RD}$  is work of friction forces (energy dissipation due to friction at the lower boundary of the upper and lower layers);  $W_{RL2}$  is work of friction forces (energy entering the lower layer from the upper due to friction between the layers);  $W_{G1}$ ,  $W_{G2}$  is pressure gradient work (transition between kinetic and potential energy in the upper and lower layers);  $W_{AB1}$ ,  $W_{AB2}$  is work of horizontal turbulent viscosity forces in layers (energy dissipation).

Flows  $W_{G1}$ ,  $W_{G2}$  with different signs enter simultaneously into the balance equations of kinetic and potential energy, thereby providing energy connection between the upper and lower layers.

Work of the Coriolis force  $W_{C1}$  and  $W_{C2}$  in equations (1) is equal to zero, but it can be non-zero separately for MCs and MEs, as it will be shown below. Therefore, these terms are retained in the equations. In this case, the Coriolis force work determines the kinetic energy transitions between the MCs and the MEs.

### Energy characteristics of MCs and MEs

Thus, the task requires to separate the energy characteristics of flows obtained using a numerical model by the scale of movement, namely: to calculate the time-average values of energy and its transitions separately for mean currents and mesoscale eddy formations. It is also necessary to determine how energy is exchanged between MCs and MEs. The separate calculations will be carried out for the eastern and western parts of the sea.

Consideration of average characteristics permits to exclude time derivatives of energy in the energy balance equations so that to reduce the number of factors influencing the variability of energy characteristics. This somewhat simplifies the analysis.

Let us rewrite equations (1) averaged over a long period of time in terms of energy transitions using construction  $\{E_1, E_2\}$  to denote the time-average transition of one energy type to another [21]. If  $\{E_1, E_2\} > 0$ , this means that  $E_2$  goes into  $E_1$ , and vice versa: if  $\{E_1, E_2\} < 0$ , then  $E_1$  goes into  $E_2$ :

$$\left\{ \begin{array}{l} \frac{\partial \overline{U_1 e_{K1}}}{\partial x} + \frac{\partial \overline{V_1 e_{K1}}}{\partial y} = \overline{W_{C1}} + \{K_1, P\} + \{K_1, \tau\} + \{K_1, D_L\} + \{K_1, D_{T1}\}, \\ \frac{\partial \overline{U_2 e_{K2}}}{\partial x} + \frac{\partial \overline{V_2 e_{K2}}}{\partial y} = \overline{W_{C2}} + \{K_2, P\} + \{K_2, K_1\} + \{K_1, D_H\} + \{K_1, D_{T2}\}, \\ -\rho g' \left( \frac{\partial \overline{U_2 h_1}}{\partial x} + \frac{\partial \overline{V_2 h_1}}{\partial y} \right) - \rho g \left( \frac{\partial \overline{U \zeta}}{\partial x} + \frac{\partial \overline{V \zeta}}{\partial y} \right) = -\{K_1, P\} - \{K_2, P\}, \end{array} \right. \quad (2)$$

where  $\overline{W_{C1}} = 0$ ;  $\overline{W_{C2}} = 0$ ;  $\{K_1, \tau\} = \overline{W_\tau}$ ;  $\{K_1, P\} = \overline{W_{G1}}$ ;  $\{K_2, P\} = \overline{W_{G2}}$ ;  $\{K_1, D_L\} = \overline{W_{RL1}}$ ;  $\{K_2, K_1\} = \overline{W_{RL2}}$ ;  $\{K_1, D_H\} = \overline{W_{RD}}$ ;  $\{K_1, D_{T1}\} = \overline{W_{AB1}}$ ;  $\{K_1, D_{T2}\} = \overline{W_{AB2}}$ ;  $D_L$  is dissipation due to friction at the lower boundary of the upper layer;  $D_H$  is dissipation due to bottom friction;  $D_{T1}$ ,  $D_{T2}$  is dissipation due to horizontal turbulent viscosity in the upper and lower layers; the overline means averaging over time.

Let us integrate equations (2) over space within the western and eastern regions, after which we obtain two systems of equations in which square brackets with the superscript W or E indicating the region of integration are used to write the energy characteristics total over the area:

$$\begin{aligned}
 [...]^W &= \iint_W (...) dx dy, & [...]^E &= \iint_E (...) dx dy, \\
 \left\{ \begin{aligned}
 \iint_W \left( \frac{\partial \overline{U_1 e_{K1}}}{\partial x} + \frac{\partial \overline{V_1 e_{K1}}}{\partial y} \right) dx dy &= [W_{C1}]^W + [K_1, P]^W + [K_1, \tau]^W + [K_1, D_L]^W + [K_1, D_{T1}]^W, \\
 \iint_W \left( \frac{\partial \overline{U_2 e_{K2}}}{\partial x} + \frac{\partial \overline{V_2 e_{K2}}}{\partial y} \right) dx dy &= [W_{C2}]^W + [K_2, P]^W + [K_2, K_1]^W + [K_1, D_H]^W + [K_1, D_{T2}]^W, \\
 \iint_W \left( -\rho g' \left( \frac{\partial \overline{U_2 h_1}}{\partial x} + \frac{\partial \overline{V_2 h_1}}{\partial y} \right) - \rho g \left( \frac{\partial \overline{U \zeta}}{\partial x} + \frac{\partial \overline{V \zeta}}{\partial y} \right) \right) dx dy &= -[K_1, P]^W - [K_2, P]^W,
 \end{aligned} \right. \quad (3) \\
 \left\{ \begin{aligned}
 \iint_E \left( \frac{\partial \overline{U_1 e_{K1}}}{\partial x} + \frac{\partial \overline{V_1 e_{K1}}}{\partial y} \right) dx dy &= [W_{C1}]^E + [K_1, P]^E + [K_1, \tau]^E + [K_1, D_L]^E + [K_1, D_{T1}]^E, \\
 \iint_E \left( \frac{\partial \overline{U_2 e_{K2}}}{\partial x} + \frac{\partial \overline{V_2 e_{K2}}}{\partial y} \right) dx dy &= [W_{C2}]^E + [K_2, P]^E + [K_2, K_1]^E + [K_1, D_H]^E + [K_1, D_{T2}]^E, \\
 \iint_E \left( -\rho g' \left( \frac{\partial \overline{U_2 h_1}}{\partial x} + \frac{\partial \overline{V_2 h_1}}{\partial y} \right) - \rho g \left( \frac{\partial \overline{U \zeta}}{\partial x} + \frac{\partial \overline{V \zeta}}{\partial y} \right) \right) dx dy &= -[K_1, P]^E - [K_2, P]^E.
 \end{aligned} \right. \quad (4)
 \end{aligned}$$

Using the divergence theorem and the no-slip conditions on a solid boundary, the double area integrals are replaced from the divergence of advective energy flows on the left side of the equations with linear integrals from the  $x$ -component of these flows along boundary  $D$ :

$$\begin{aligned}
 \int_D \overline{F_{K1}}(y) dy &= \iint_W \left( \frac{\partial \overline{U_1 e_{K1}}}{\partial x} + \frac{\partial \overline{V_1 e_{K1}}}{\partial y} \right) dx dy = - \iint_E \left( \frac{\partial \overline{U_1 e_{K1}}}{\partial x} + \frac{\partial \overline{V_1 e_{K1}}}{\partial y} \right) dx dy, \\
 \int_D \overline{F_{K2}}(y) dy &= \iint_W \left( \frac{\partial \overline{U_2 e_{K2}}}{\partial x} + \frac{\partial \overline{V_2 e_{K2}}}{\partial y} \right) dx dy = - \iint_E \left( \frac{\partial \overline{U_2 e_{K2}}}{\partial x} + \frac{\partial \overline{V_2 e_{K2}}}{\partial y} \right) dx dy, \\
 \int_D \overline{F_P}(y) dy &= \iint_E \left( -\rho g' \left( \frac{\partial \overline{U_2 h_1}}{\partial x} + \frac{\partial \overline{V_2 h_1}}{\partial y} \right) - \rho g \left( \frac{\partial \overline{U \zeta}}{\partial x} + \frac{\partial \overline{V \zeta}}{\partial y} \right) \right) dx dy = \\
 &= - \iint_W \left( -\rho g' \left( \frac{\partial \overline{U_2 h_1}}{\partial x} + \frac{\partial \overline{V_2 h_1}}{\partial y} \right) - \rho g \left( \frac{\partial \overline{U \zeta}}{\partial x} + \frac{\partial \overline{V \zeta}}{\partial y} \right) \right) dx dy,
 \end{aligned} \quad (5)$$

where  $\overline{F_{K1}} = \overline{U_1 e_{K1}}$ ,  $\overline{F_{K2}} = \overline{U_1 e_{K1}}$ ,  $\overline{F_p} = -\rho \left( g' \overline{U_2 h_1} + g \overline{(U_1 + U_2) \zeta} \right)$  are average advective flows of kinetic and potential energy between the western and eastern parts of the sea.

To divide the energy characteristics according to the movement scale, the above definition for MC and ME will be used. As already mentioned, MC is obtained by averaging instantaneous current fields over time, and ME is the deviation of instantaneous currents from MC. Superscript m is used to identify MC and its energy characteristics, and superscript p is used for ME.

Mathematically, the division of circulation according to the movement scale can be expressed through currents (water flows) in the layers as follows:

$$\begin{aligned} U_1 &= U_1^m + U_1^p = \overline{u_1 h_1} + (u_1 h_1)', & V_1 &= V_1^m + V_1^p = \overline{v_1 h_1} + (v_1 h_1)', \\ U_2 &= U_2^m + U_2^p = \overline{u_2 h_2} + (u_2 h_2)', & V_2 &= V_2^m + V_2^p = \overline{v_2 h_2} + (v_2 h_2)', \end{aligned} \quad (6)$$

where the prime symbol means a deviation (pulsation) from the average value;  $(U_1, V_1)$ ,  $(U_2, V_2)$  are components of currents (flows) in layers;  $(U_1^m, V_1^m)$ ,  $(U_2^m, V_2^m)$  are components of the mean current;  $(U_1^p, V_1^p)$ ,  $(U_2^p, V_2^p)$  are components of pulsation flows, or MEs.

In the present paper, the current averaging period was chosen equal to the averaging period of equations (2).

If expressions (6) are substituted into system of equations (1), then after opening the brackets and dividing the terms of the equations according to the scale of motion, separate systems of energy balance equations for MC and ME will be obtained.

Let us show how separation by scale of motion works using the example of the term that describes the work of the Coriolis force in the first equation of system (1):

$$\begin{aligned} W_{C1} &= u_1 h_1 \cdot f v_1 - v_1 h_1 \cdot f u_1 = (U_1^m + U_1^p) \cdot f v_1 - (V_1^m + V_1^p) \cdot f u_1, \\ W_{C1} &= (U_1^m \cdot f v_1 - V_1^m \cdot f u_1) + (U_1^p \cdot f v_1 - V_1^p \cdot f u_1) = W_{C1}^m + W_{C1}^p, \end{aligned}$$

where  $W_{C1}^m = U_1^m \cdot f v_1 - V_1^m \cdot f u_1$  and  $W_{C1}^p = U_1^p \cdot f v_1 - V_1^p \cdot f u_1$  is work of the Coriolis force, carried out by MC and ME, respectfully.

Fig. 3 shows the vector of the instantaneous flow decomposed into the mean and pulsating flows, and the vector of the Coriolis force acting on the instantaneous flow.

According to the figure, the division of currents (flows) into mean (MCs) and pulsating (MEs) leads to the appearance of non-zero values of the Coriolis force work associated with them. In total, these values are equal to zero, i.e., they cancel each other out. However, when dividing the energy balance equations for real flows into equations for MC and ME, the corresponding Coriolis force work should be taken into account to harmonize the systems of equations. It is correct to consider this work imaginary (fictitious), since the division of flows into mean and pulsating ones is also imaginary, existing only within the framework of the representation method used.

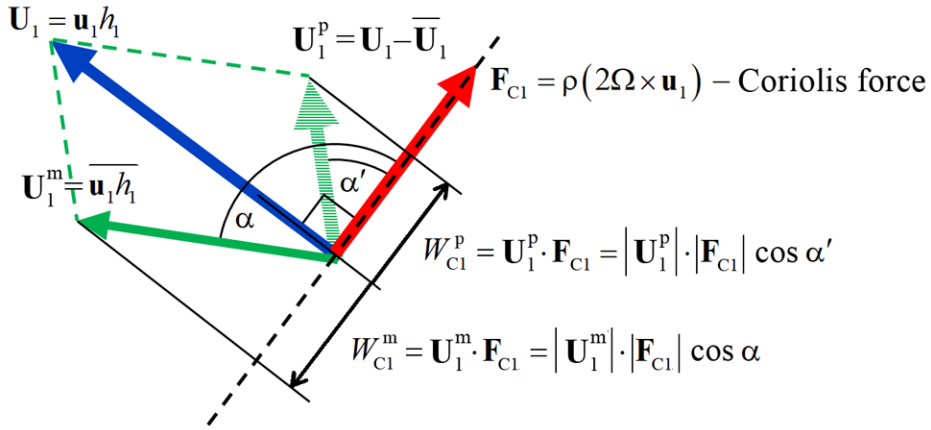


**Fig. 3.** Appearance of non-zero values of the Coriolis force work ( $W_{Ci}^m = -W_{Ci}^p \neq 0$ ) at decomposing the flows into a sum of the average  $\overline{u_1 h_1}$  and pulsation  $(u_1 h_1)'$  values

In the energy balance equations of MC and ME, the Coriolis force work determines the transitions of kinetic energy between mean and pulsating flows. It can be said that mean and pulsating flows that do not actually exist exchange kinetic energy with each other due to the imaginary Coriolis force work, which itself is an imaginary (fictitious) force.

Considering that equations (3)–(5) are a consequence of equations (1), two systems of equations in which the terms related to MC and ME are separated into different equations for the western and eastern parts of the Black Sea are obtained:

$$\left\{ \begin{array}{l} \Phi_{K_1}^m = [K_1^m, K_1^p]^W + [K_1^m, P^m]^W + [K_1^m, \tau]^W + [K_1^m, D_L^m]^W + [K_1^m, D_{T1}^m]^W, \\ \Phi_{K_1}^p = [K_1^p, K_1^m]^W + [K_1^p, P^p]^W + [K_1^p, \tau]^W + [K_1^p, D_L^p]^W + [K_1^p, D_{T1}^p]^W, \\ \Phi_{K_2}^m = [K_2^m, K_2^p]^W + [K_2^m, P^m]^W + [K_2^m, K_1^m]^W + [K_2^m, D_H^m]^W + [K_2^m, D_{T2}^m]^W, \\ \Phi_{K_2}^p = [K_2^p, K_2^m]^W + [K_2^p, P^p]^W + [K_2^p, K_1^p]^W + [K_2^p, D_H^p]^W + [K_2^p, D_{T2}^p]^W, \\ \Phi_P^m = -[K_1^m, P^m]^W - [K_2^m, P^m]^W, \\ \Phi_P^p = -[K_1^p, P^p]^W - [K_2^p, P^p]^W, \end{array} \right. \quad (7)$$

$$\left\{ \begin{array}{l} -\Phi_{K_1}^m = [K_1^m, K_1^p]^E + [K_1^m, P^m]^E + [K_1^m, \tau]^E + [K_1^m, D_L^m]^E + [K_1^m, D_{T1}^m]^E, \\ -\Phi_{K_1}^p = [K_1^p, K_1^m]^E + [K_1^p, P^p]^E + [K_1^p, \tau]^E + [K_1^p, D_L^p]^E + [K_1^p, D_{T1}^p]^E, \\ -\Phi_{K_2}^m = [K_2^m, K_2^p]^E + [K_2^m, P^m]^E + [K_2^m, K_1^m]^E + [K_2^m, D_H^m]^E + [K_2^m, D_{T2}^m]^E, \\ -\Phi_{K_2}^p = [K_2^p, K_2^m]^E + [K_2^p, P^p]^E + [K_2^p, K_1^p]^E + [K_2^p, D_H^p]^E + [K_2^p, D_{T2}^p]^E, \\ -\Phi_P^m = -[K_1^m, P^m]^E - [K_2^m, P^m]^E, \\ -\Phi_P^p = -[K_1^p, P^p]^E - [K_2^p, P^p]^E, \end{array} \right. \quad (8)$$

$$\begin{aligned}
& \text{where } \Phi_{K_1}^m = \int_D F_{K_1}^m dy; \Phi_{K_2}^m = \int_D F_{K_2}^m dy; \Phi_P^m = \int_D F_P^m dy; \Phi_{K_1}^p = \int_D F_{K_1}^p dy; \\
& \Phi_{K_2}^p = \int_D F_{K_2}^p dy; \Phi_P^p = \int_D F_P^p dy; F_{K_1}^m + F_{K_1}^p = \overline{F_{K_1}}; F_{K_2}^m + F_{K_2}^p = \overline{F_{K_2}}; F_P^m + F_P^p = \overline{F_P}; \\
& F_{K_1}^m = U_1^m \cdot \overline{e_{K_1}}; F_{K_1}^p = \overline{F_{K_1}} - F_{K_1}^m; F_{K_2}^m = U_2^m \cdot \overline{e_{K_2}}; F_{K_2}^p = \overline{F_{K_2}} - F_{K_2}^m; \\
& F_P^m = -\rho(g'U_2^m \cdot \overline{h_1} + g(U_1^m + U_2^m)\overline{\zeta}); F_P^p = \overline{F_P} - F_P^m; \\
& [K_1^m, K_1^p]^W = [W_{C1}^m]^W = [U_1^m \cdot f \overline{v_1} - V_1^m \cdot f \overline{u_1}]^W; \\
& [K_1^p, K_1^m]^W = [W_{C1}^p]^W = -[K_1^m, K_1^p]^W; [K_1^m, P^m]^W = \rho g [U_1^m \cdot \overline{\zeta_x} + V_1^m \cdot \overline{\zeta_y}]^W; \\
& [K_1^p, P^p]^W = \rho g [\overline{U_1 \zeta_x} + \overline{V_1 \zeta_y}]^W - [K_1^m, P^m]^W; \\
& [K_1^m, \tau]^W = \rho [U_1^m \cdot \overline{\tau^x h_1^{-1}} + V_1^m \cdot \overline{\tau^y h_1^{-1}}]^W; [K_1^p, \tau]^W = \rho [\overline{u_1 \tau^x} + \overline{v_1 \tau^y}]^W - [K_1^m, \tau]^W; \\
& [K_1^m, D_L^m]^W = \rho [U_1^m \cdot \overline{R_{L1}^x h_1^{-1}} + V_1^m \cdot \overline{R_{L1}^y h_1^{-1}}]^W; \\
& [K_1^p, D_L^p]^W = \rho [\overline{u_1 R_{L1}^x} + \overline{v_1 R_{L1}^y}]^W - [K_1^m, D_L^m]^W; \\
& [K_1^m, D_{T1}^m]^W = \rho A_B [U_1^m (\Delta \Delta \overline{u_1}) + V_1^m (\Delta \Delta \overline{v_1})]^W; \\
& [K_1^p, D_{T1}^p]^W = \rho A_B [\overline{U_1 (\Delta \Delta u_1)} + \overline{V_1 (\Delta \Delta v_1)}]^W - [K_1^m, D_{T1}^m]^W; \\
& [K_2^m, K_2^p]^W = [W_{C2}^m]^W = [U_2^m \cdot f \overline{v_2} - V_2^m \cdot f \overline{u_2}]^W; \\
& [K_2^p, K_2^m]^W = [W_{C2}^p]^W = -[K_2^m, K_2^p]^W; \\
& [K_2^m, P^m]^W = \rho [g(U_2^m \cdot \overline{\zeta_x} + V_2^m \cdot \overline{\zeta_y}) + g'(U_2^m \cdot \overline{h_{1x}} + V_2^m \cdot \overline{h_{1y}})]^W; \\
& [K_2^p, P^p]^W = \rho [g(\overline{U_2 \zeta_x} + \overline{V_2 \zeta_y}) + g'(\overline{U_2 h_{1x}} + \overline{V_2 h_{1y}})]^W - [K_2^m, P^m]^W; \\
& [K_2^m, K_1^m]^W = \rho [U_2^m \cdot \overline{R_{L2}^x h_2^{-1}} + V_2^m \cdot \overline{R_{L2}^y h_2^{-1}}]^W; \\
& [K_2^p, K_1^p]^W = \rho [\overline{u_2 R_{L2}^x} + \overline{v_2 R_{L2}^y}]^W - [K_2^m, K_1^m]^W; \\
& [K_2^m, D_H^m]^W = \rho [U_2^m \cdot \overline{R_D^x h_2^{-1}} + V_2^m \cdot \overline{R_D^y h_2^{-1}}]^W; \\
& [K_2^p, D_H^p]^W = \rho [\overline{u_2 R_D^x} + \overline{v_2 R_D^y}]^W - [K_2^m, D_H^m]^W; \\
& [K_2^m, D_{T2}^m]^W = \rho A_B [U_2^m (\Delta \Delta \overline{u_2}) + V_2^m (\Delta \Delta \overline{v_2})]^W; \\
& [K_2^p, D_{T2}^p]^W = \rho A_B [\overline{U_2 (\Delta \Delta u_2)} + \overline{V_2 (\Delta \Delta v_2)}]^W - [K_2^m, D_{T2}^m]^W.
\end{aligned}$$

Formulas for calculating energy transitions in the eastern part of the sea are obtained by replacing  $W$  with  $E$  in the expressions above.

Expressions  $[K_1^m, K_1^p]^W$ ,  $[K_1^p, K_1^m]^W$ ,  $[K_2^m, K_2^p]^W$ ,  $[K_2^p, K_2^m]^W$ ,  $[K_1^m, K_1^p]^E$ ,  $[K_1^p, K_1^m]^E$ ,  $[K_2^m, K_2^p]^E$  and  $[K_2^p, K_2^m]^E$  are not equal to zero and determine the transitions of kinetic energy between MC and ME in the corresponding part of the sea.

### Calculation results of energy characteristics

First of all, the time-average energy values of large-scale currents and mesoscale eddy formations in the western and eastern parts of the sea were determined, for which formulas for  $K_1$ ,  $K_2$ ,  $P$ , expressions (6) and representation  $h_1 = h_1^m + h_1^p$  (where  $h_1^m = \bar{h}_1$ ) were used:

$$K_1 = h_1 e_{K1} = \rho \frac{h_1 u_1^2 + h_1 v_1^2}{2} = \rho \frac{(U_1^m u_1 + V_1^m v_1) + (U_1^p u_1 + V_1^p v_1)}{2},$$

$$K_2 = h_2 e_{K2} = \rho \frac{h_2 u_2^2 + h_2 v_2^2}{2} = \rho \frac{(U_2^m u_2 + V_2^m v_2) + (U_2^p u_2 + V_2^p v_2)}{2},$$

$$P = \rho g' \frac{h_1^2 - h_0^2}{2} = \rho g' \frac{(h_1^m + h_1^p)^2 - h_0^2}{2} = \rho g' \frac{(h_1^m)^2 + 2h_1^m h_1^p + (h_1^p)^2 - h_0^2}{2}.$$

Averaging over time and dividing by scale of motion gives

$$\overline{K_1} = \rho \frac{(U_1^m \bar{u}_1 + V_1^m \bar{v}_1) + \overline{(U_1^p u_1 + V_1^p v_1)}}{2} = \rho \frac{(U_1^m \bar{u}_1 + V_1^m \bar{v}_1)}{2} + \rho \frac{\overline{(U_1^p u_1 + V_1^p v_1)}}{2},$$

$$\overline{K_1} = K_1^m + K_1^p, \quad K_1^m = \rho \frac{U_1^m \bar{u}_1 + V_1^m \bar{v}_1}{2}, \quad K_1^p = \rho \frac{\overline{(U_1^p u_1 + V_1^p v_1)}}{2} = \overline{K_1} - K_1^m,$$

$$\overline{K_2} = \rho \frac{(U_2^m \bar{u}_2 + V_2^m \bar{v}_2) + \overline{(U_2^p u_2 + V_2^p v_2)}}{2} = \rho \frac{(U_2^m \bar{u}_2 + V_2^m \bar{v}_2)}{2} + \rho \frac{\overline{(U_2^p u_2 + V_2^p v_2)}}{2},$$

$$\overline{K_2} = K_2^m + K_2^p, \quad K_2^m = \rho \frac{U_2^m \bar{u}_2 + V_2^m \bar{v}_2}{2}, \quad K_2^p = \rho \frac{\overline{(U_2^p u_2 + V_2^p v_2)}}{2} = \overline{K_2} - K_2^m,$$

$$\overline{P} = \rho g' \frac{(h_1^m)^2 - h_0^2 + \overline{(h_1^p)^2}}{2} = \rho g' \frac{(h_1^m)^2 - h_0^2}{2} + \rho g' \frac{\overline{(h_1^p)^2}}{2},$$

$$\overline{P} = P^m + P^p, \quad P^m = \rho g' \frac{(h_1^m)^2 - h_0^2}{2}, \quad P^p = \rho g' \frac{\overline{(h_1^p)^2}}{2} = \overline{P} - P^m.$$

After integrating the time-averaged MC and ME energies over the area for the western and eastern parts of the sea, the required values are obtained (see Table).

**Time-averaged kinetic and available potential energy (TJ)**

$[K_1]$	$[K_2^m]$	$[K_1^p]$	$[K_2]$	$[K_2^m]$	$[K_2^p]$	$[P]$	$[P^m]$	$[P^p]$
<i>Western part</i>								
313.7	238.3	75.4	48.4	1.9	46.4	881.1	756.0	125.0
<i>Eastern part</i>								
370.7	286.6	84.1	61.7	2.2	59.4	2915.0	2773.2	141.8

Time-averaged energies are stationary and do not affect energy transitions, but their knowledge is useful for a general understanding of the Black Sea energy and comparison of modelling results with observational data.

According to the data obtained, the MC and ME kinetic energy is distributed in the Black Sea quite evenly between its eastern and western parts. Slightly higher values of kinetic energy in the eastern part can be explained by the greater extent of large-scale currents in this part of the basin.

In the upper layer, the kinetic energy of MC is approximately three times greater than this of ME, and it is the other way around in the lower layer: ME contains 25 times more kinetic energy than MC.

Most of the average mechanical energy in the sea (~ 60%) falls on the available potential energy of MC concentrated in its eastern half. It is almost 10 times greater than the kinetic energy of MC in this part of the basin. In the western part, the total available potential energy of MC is three times higher than its kinetic energy. Moreover, it is three times less than the available potential energy of MC in the eastern part.

For ME, the difference in the  $P$  distribution between the western and eastern parts is proportional to the length of the average Rim Current in the corresponding area.

It is worth paying attention to the revealed pattern: in total, the kinetic energy of ME of the upper and lower layers turned out to be approximately equal to its available potential energy:

$$[K_1^p]^w + [K_2^p]^w \approx [P^p]^w, \quad [K_1^p]^e + [K_2^p]^e \approx [P^p]^e.$$

At the next stage, the average advective energy transfers between the western and eastern parts of the sea carried out by MC and ME were calculated. It is these flows resulting from the  $\beta$ -effect, as shown in [17], that are the cause of the spatial heterogeneity formation of the fields of energy characteristics in the Black Sea.

Fig. 4 shows the distribution of advective energy flows along the  $Y$  axis. In the upper layer, the maximum average transfer of kinetic energy is observed in the average Rim Current core (Fig. 4, *a*). The energy transfer direction coincides with the current direction. The main contribution to the kinetic energy advection is made by MC (Fig. 4, *b*), the maximum  $F_{K1}^m$  coincides with the mean flow core.

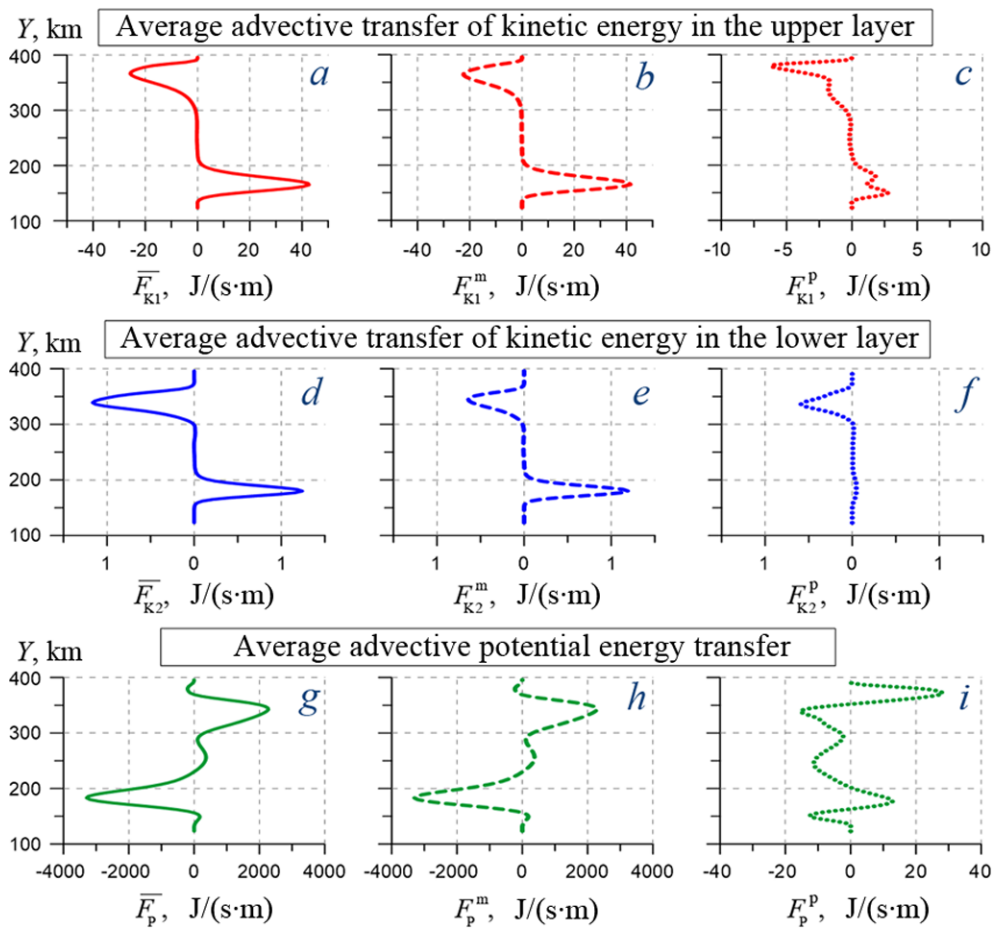


**Fig. 4.** Distribution of the energy advective flows along boundary D: mean flows are shown by a solid line, share of MCs – by a dashed line, share of MEs – by a dotted one

The southern MC branch transfers more energy than the northern one; as a result, the total flow of kinetic energy  $\Phi_{K1}^m$  is 33 MJ/s, and it is directed from the western part of the sea to the eastern one (Fig. 5, a).



**Fig. 5.** Total advective energy flows (MJ/s) between the eastern and western parts of the sea:  $\Phi_{K1}^m$ ,  $\Phi_{K1}^p$  (a);  $\Phi_{K2}^m$ ,  $\Phi_{K2}^p$  (b);  $\Phi_P^m$ ,  $\Phi_P^p$  (c)

Mesoscale eddy formations in the upper layer of the sea carry out the kinetic energy transfer in the same way as MCs, in the average Rim Current direction, but the maximum energy flows of MEs do not coincide with the average flow core, but are located next to it in the zones of the highest current velocity gradient (Fig. 4, *c*). Moreover, to the right of ME core the energy transfer is greater than to the left. Most likely, this happens because mesoscale anticyclonic eddies that are formed between the Rim Current and the coast contain more energy than cyclonic MEs that are formed mainly to the left of the Rim Current. The maximum advective flow of ME kinetic energy is observed to the right of the northern MC branch; it makes the main contribution to the total advective transport  $\Phi_{k1}^p$ , which is 14 MJ/s in the western direction (Fig. 5, *a*). This is less than  $\Phi_{k1}^m$ , therefore the total advective transfer of kinetic energy by currents in the upper layer is directed from the western half of the sea to the eastern one.

In the lower layer, the southern MC branch transports more kinetic energy in the eastern direction than the northern one in the western direction (Fig. 4, *e*). But the overall transfer of kinetic energy (Fig. 4, *d*) is still directed to the west due to the ME advective flow, which is maximum in the northern part of section D (Fig. 4, *f*). The total advective flow of kinetic MC energy  $\Phi_{k2}^m$  directed to the east is 0.4 MJ/s, and the total flow of kinetic ME energy  $\Phi_{k2}^p$  is directed to the west and is 0.5 MJ/s (Fig. 5, *b*).

The average advective transfer of potential ME energy occurs in the flow opposite direction in contrast to kinetic energy transfer (Fig. 4, *g, h*). The maximum values are noted in the MC core of the lower layer. They are much higher than the maxima of the kinetic MC energy flows in the upper and lower layers. However, the total flow in this case turns out to be of the same order of magnitude and is 25 MJ/s in the western direction due to the southern MC branch (Fig. 5, *c*).

The most interesting is the  $F_p^p$  advective flow distribution along section D (Fig. 4, *i*). Its maxima are in the MC core area in the lower layer, and it is directed along the flow. To the right of the MC core  $F_p^p$ , the flow changes direction to the opposite, reaches its maximum and becomes zero on the shore. It can be assumed that this  $F_p^p$  distribution is associated with mesoscale anticyclonic eddies formation and movement to the MC right (Fig. 1, *f*). In [9], it is shown that such eddies are elements of gradient-eddy waves (captured by the continental slope) which belong to the class of topographic Rossby waves. In general, the  $F_p^p$  flows between the MC core and the shore compensate each other due to their multidirectionality.

In the central part of section D (Fig. 4, *i*, between 200 and 300 km on the vertical scale) there is another maximum of  $F_p^p$  advective flow, which determines the main contribution of ME to the total potential energy transfer, resulting in a total flow  $\Phi_p^p = 40$  MJ/s directed to the west (Fig. 5, *c*).

In general, it can be said that MEs transfer both kinetic and potential energy from the eastern part of the Black Sea to the western one, while MCs transfer only potential energy to the west. The greatest contribution to the western energy transfer is made by the  $\Phi_p^p$  advective flow (Fig. 5, *c*), which is formed due to the potential energy transfer by mesoscale eddy formations through the central part of section D. According to [9, 22], such MEs are barotropic Rossby waves of a closed basin, formed in the deep sea due to the  $\beta$ -effect. As shown in <sup>3</sup>, in a two-layer liquid basin under stationary wind action, it is barotropic Rossby waves that are generated. If a seasonally varying wind is used to excite motion in the model, then in addition to barotropic waves, baroclinic Rossby waves <sup>3</sup> will also be formed in the basin [23].

Let us consider the time-average transitions of mechanical energy that are a consequence of dynamic processes in the sea, taking into account the division of currents into MCs and MEs. These transitions calculated for the western and eastern parts of the Black Sea are shown diagrammatically in Fig. 6. The time averaging period was 20 model years which was enough for the time variability of the average energy characteristics to be close to zero.

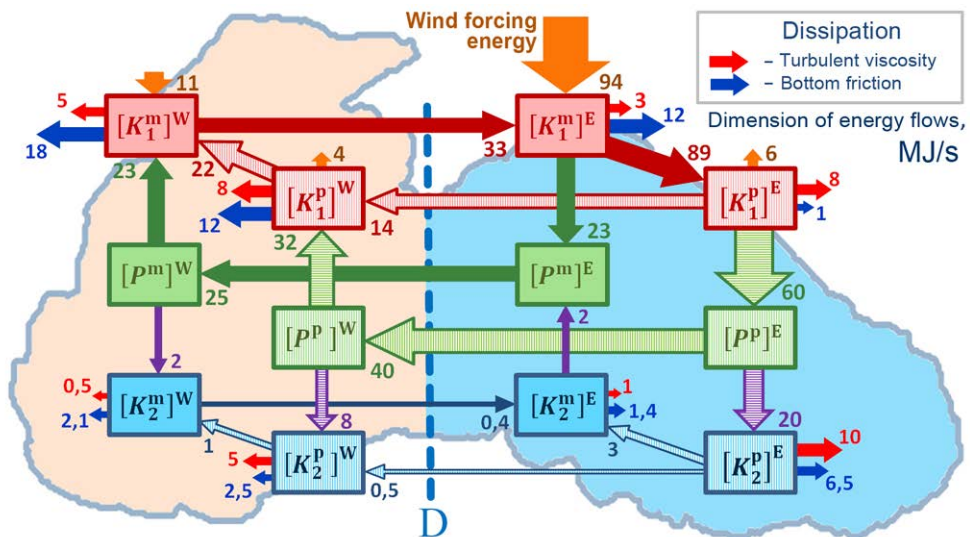


**Fig. 6.** Mean energy flows between the mean currents and the mesoscale eddies with regard to the sea division into two parts – the western and eastern ones

<sup>3</sup> Safronov, G.F., 1985. [Excitation of Long Waves in the Ocean by Large-Scale Changes in the Tangential Wind Stress Field]. Moscow: Gidrometeoizdat, 108 p. (in Russian).

Let us note a number of features in energy transitions.

1. Wind energy pumping is observed mainly in the eastern part of the sea (94 MJ/s), which is explained by the wind field features used in the model and corresponds to observations [14]. In the western part, the wind energy influx is 11 MJ/s, which is 9 times less than in the eastern part.

2. All the energy coming from the wind goes to replenish the kinetic MC energy in the upper layer. The wind has an average braking effect on MEs, which leads to a loss of kinetic ME energy in both eastern (6 MJ/s) and western (4 MJ/s) parts of the sea.

3. MEs get kinetic energy from MCs in the upper layer of the eastern part of the sea, and a reverse transition of kinetic energy from MEs to MCs is observed in the western part.

4. The MC and ME kinetic energy transforms into the potential MC and ME energy in the upper layer of the eastern part of the sea, in the western part there is the opposite direction of energy transitions from potential to kinetic one.

5. Energy enters the lower layer of the sea due to the transition of the available potential ME energy into the kinetic ME energy in both eastern and western parts.

6. The kinetic MC energy of the lower layer in both parts of the sea is replenished by the kinetic ME energy, i.e., a transition of energy from small-scale movements to larger ones is observed. Such an energy transition is called the effect of negative viscosity in the theory of turbulence, but in this case it is the result of averaging of trapped waves moving over the continental slope, which transport a certain mass of water due to nonlinearity, i.e., have the properties of eddies.

7. Part of the kinetic MC energy of the lower layer transforms into the potential MC energy in the eastern half of the sea, and in the western one – vice versa: the potential MC energy partially transforms into the kinetic MC energy.

8. Despite the fact that the energy influx into the sea takes place predominantly in its eastern part, energy dissipation in the west is greater than in the east (53 and 42 MJ/s, respectively). Moreover, the most energy (67 MJ/s) is lost due to dissipation in the upper layer, with 43 MJ/s occurring in the western part of the sea.

Fig. 6 does not indicate the kinetic energy transitions from the upper layer to the lower one due to their smallness. The corresponding values are taken into account in the energy dissipation.

An important feature of the scheme presented, linking all its elements together, is the presence of the advective energy flows discussed above, directed from one part of the sea to the other (Fig. 5). On the one hand, it can be said that these advective flows compensate for differences in the size and direction of energy transitions in the western and eastern parts. On the other hand, these advective energy flows, being a consequence of the  $\beta$ -effect, are the main reason for the uneven distribution of energy transitions across the sea.

## Conclusion

Consideration of the energy characteristics separately for the eastern and western parts of the Black Sea made it possible to identify a number of patterns in

the two-layer model energy and obtain new information about the course of dynamic processes in the sea. In particular, it turned out that the direction and size of mechanical energy transitions averaged over a long period of time among its types in different parts of the sea were significantly different from each other.

Differences in the direction and size of energy flows in the eastern and western parts were established. They were caused by advective energy flows, which in total are directed from the eastern half of the sea to the western one. As a result of calculating the contribution of average currents and mesoscale eddy formations to time-average advective energy flows, it was found that the main contribution to the western energy transfer was made by MEs localized in the central part outside the zone of large-scale currents distribution. On this basis, it was concluded that these MEs are Rossby waves formed as a result of the  $\beta$ -effect in a closed (bounded) basin. This conclusion confirms the  $\beta$ -effect importance for the formation of the Black Sea circulation once again.

The role of the Coriolis force work in the transitions of kinetic energy between MC and ME is shown. Thus, a reasonable question arises – how is this possible? It is known that the Coriolis force is an imaginary force and does not produce work. To resolve this contradiction, let us recall that the division of flows into MCs and MEs is artificial, or imaginary, and therefore the energy transitions between them are imaginary. These imaginary transitions are determined by the imaginary Coriolis force work which is equal to zero for total flows, but turned out to be non-zero separately for MCs and MEs.

At this stage of the research, energy characteristics averaged in a statistically equilibrium mode were analyzed over a long period of time, in which all average characteristics and model parameters remain constant. This approach simplifies energy analysis greatly, since it permits to eliminate time derivatives in the energy balance equations. At the same time, some important processes that are stochastic or periodic in their nature and are observed in different parts of the sea (e.g., baroclinic instability) are excluded from consideration. To study such processes when determining the average circulation, it is necessary to select the appropriate averaging period and take into account the spatiotemporal localization of the phenomenon itself. Further research is planned in this direction.

#### REFERENCES

1. Ivanov, V.A. and Belokopytov, V.N., 2013. *Oceanography of the Black Sea*. Sevastopol: ECOSY-Gidrofizika, 210 p.
2. Korotaev, G., Oguz, T., Nikiforov, A. and Koblinsky, C., 2003. Seasonal, Interannual, and Mesoscale Variability of the Black Sea Upper Layer Circulation Derived from Altimeter Data. *Journal of Geophysical Research: Oceans*, 108(C4), 3122. doi:10.1029/2002JC001508
3. Korotenko, K.A., 2015. Modeling Mesoscale Circulation of the Black Sea. *Oceanology*, 55(6), pp. 820-826. doi:10.1134/S0001437015060077
4. Zhang, Z., Zhang, Y., Wang, W. and Huang, R.X., 2013. Universal Structure of Mesoscale Eddies in the Ocean. *Geophysical Research Letters*, 40(14), pp. 3677-3681. doi:10.1002/grl.50736

5. Chelton, D.B., Schlax, M.G. and Samelson, R.M., 2011. Global Observations of Nonlinear Mesoscale Eddies. *Progress in Oceanography*, 91(2), pp. 167-216. doi:10.1016/j.pcean.2011.01.002
6. Chen, G., Hou, Y. and Chu, X., 2011. Mesoscale Eddies in the South China Sea: Mean Properties, Spatiotemporal Variability, and Impact on Thermohaline Structure. *Journal of Geophysical Research: Oceans*, 116(C6), C06018. doi:10.1029/2010JC006716
7. Kubryakov, A.A. and Stanichny, S.V., 2015. Mesoscale Eddies in the Black Sea from Satellite Altimetry Data. *Oceanology*, 55(1), pp. 56-67. doi:10.1134/S0001437015010105
8. Kantha, L.H. and Clayson, C.A., eds., 2000. *Numerical Models of Oceans and Oceanic Processes*. International Geophysics Series, vol. 66. San-Diego: Academic Press, 940 p. doi:10.1016/s0074-6142(00)x8001-1
9. Pavlushin, A.A., Shapiro, N.B. and Mikhailova, E.N., 2017. The Role of the Bottom Relief and the  $\beta$ -Effect in the Black Sea Dynamics. *Physical Oceanography*, (6), pp. 24-35. doi:10.22449/1573-160X-2017-6-24-35
10. Zatsepin, A.G., Baranov, V.I., Kondrashov, A.A., Korzh, A.O., Kremenetskiy, V.V., Ostrovskii, A.G. and Soloviev, D.M., 2011. Submesoscale Eddies at the Caucasus Black Sea Shelf and the Mechanisms of their Generation. *Oceanology*, 51(4), pp. 554-567. doi:10.1134/S0001437011040205
11. Capet, X., McWilliams, J.C., Molemaker, M.J. and Shchepetkin, A.F., 2008. Mesoscale to Submesoscale Transition in the California Current System. Part II: Frontal Processes. *Journal of Physical Oceanography*, 38(1), pp. 44-64. doi:10.1175/2007JPO3672.1
12. Kubryakov, A.A., Lishaev, P.N., Chepyzhenko, A.I., Aleskerova, A.A., Kubryakova, E.A., Medvedeva, A.V. and Stanichny, S.V., 2021. Impact of Submesoscale Eddies on the Transport of Suspended Matter in the Coastal Zone of Crimea Based on Drone, Satellite, and in Situ Measurement Data. *Oceanology*, 61(2), pp. 159-172. doi:10.1134/S0001437021020107
13. Kalashnik, M.V., Kurganskii, M.V. and Chkhetiani, O.G., 2022. Baroclinic Instability in Geophysical Fluid Dynamics. *Physics-Uspekhi*, 65(10), pp. 1039-1070. doi:10.3367/UFNe.2021.08.039046
14. Zatsepin, A.G., Kremenetskiy, V.V., Stanichny, S.V. and Burdyugov, V.M., 2010. Black Sea Basin-Scale Circulation and Mesoscale Dynamics under Wind Forcing. In: A. V. Frolov and Yu. D. Resnyansky, eds., 2010. *Modern Problems of Ocean and Atmosphere Dynamics. The Pavel S. Lineykin Memorial Volume*. Moscow: Triada Ltd., pp. 347-368 (in Russian).
15. Kang, D. and Curchitser, E.N., 2015. Energetics of Eddy-Mean Flow Interactions in the Gulf Stream Region. *Journal of Physical Oceanography*, 45(4), pp. 1103-1120. doi:10.1175/JPO-D-14-0200.1
16. Demyshev, S.G. and Dymova, O.A., 2022. Analysis of the Lorenz Energy Cycle for Different Regimes of the Black Sea Circulation. *Transactions of the Karelian Research Centre RAS*, (6), pp. 26-40. doi:10.17076/lim1621 (in Russian).
17. Pavlushin, A.A., 2023. Features and Reasons for Spatial Heterogeneity of Mechanical Energy Flows in the Black Sea. *Physical Oceanography*, 30(3), pp. 302-314. doi:10.29039/1573-160X-2023-3-302-314
18. Pavlushin, A.A., Shapiro, N.B. and Mikhailova, E.N., 2019. Trapped Waves and the Rim Current Meandering. *Ecological Safety of Coastal and Shelf Zones of Sea*, (4), pp. 14-21. doi:10.22449/2413-5577-2019-4-14-21 (in Russian).
19. Markova, N.V. and Bagaev, A.V., 2016. The Black Sea Deep Current Velocities Estimated from the Data of Argo Profiling Floats. *Physical Oceanography*, (3), pp. 23-35. doi:10.22449/1573-160X-2016-3-23-35

20. Klyuvitkin, A.A., Ostrovskii, A.G., Lisitzin, A.P. and Konovalov, S.K., 2019. The Energy Spectrum of the Current Velocity in the Deep Part of the Black Sea. *Doklady Earth Sciences*, 488(2), pp. 1222-1226. doi:10.1134/S1028334X1910012X
21. Holland, W.R. and Lin, L.B., 1975. On the Generation of Mesoscale Eddies and Their Contribution to the Oceanic General Circulation. I. A Preliminary Numerical Experiment. *Journal of Physical Oceanography*, 5(4), pp. 642-657. doi:10.1175/1520-0485(1975)005<0642:OTGOME>2.0.CO;2
22. Stanev, E.V. and Rachev, N.H., 1999. Numerical Study on the Planetary Rossby Modes in the Black Sea. *Journal of Marine Systems*, 21(1-4), pp. 283-306. doi:10.1016/S0924-7963(99)00019-6
23. Pavlushin, A.A., 2022. Self-Oscillations of Large-Scale Circulation Intensity in the Black Sea. *Physical Oceanography*, 29(6), pp. 587-601. doi:10.22449/1573-160X-2022-6-587-601

Submitted 31.12.2022; approved after review 22.06.2023;  
accepted for publication 15.11.2023.

*About the author:*

**Andrey A. Pavlushin**, Junior Research Associate, Marine Hydrophysical Institute of RAS (2 Kapitanskaya Str., Sevastopol, 299011, Russian Federation), **ORCID ID: 0000-0002-2098-5068**, **ResearcherID: R-4908-2018**, pavlushin@mhi-ras.ru

*The author has read and approved the final manuscript.*

*The author declares that he has no conflict of interest.*